Pharm Res (2013) 30:538–551
DOI 10.1007/s11095-012-0899-x

RESEARCH PAPER

Lecithin-Based Microemulsions for Targeted Delivery of Ceramide AP into the Stratum Corneum: Formulation, Characterizations, and *In Vitro* Release and Penetration Studies

Fitsum F. Sahle • Hendrik Metz • Johannes Wohlrab • Reinhard H. H. Neubert

Received: 4 August 2012 / Accepted: 8 October 2012 / Published online: 8 November 2012

ABSTRACT

Purpose To improve the solubility and penetration of Ceramide AP (CER [AP]) into the stratum corneum that potentially restores the barrier function of aged and affected skin.

Methods CER [AP] microemulsions (MEs) were formulated using lecithin, Miglyol® 812 (miglyol) and water-1,2 pentandiol (PeG) mixture as amphiphilic, oily and hydrophilic components, respectively. The nanostructure of the MEs was revealed using electrical conductivity, differential scanning calorimeter (DSC) and electron paramagnetic resonance (EPR) techniques. Photon correlation spectroscopy (PCS) was used to measure the sizes and shape of ME droplets. The release and penetration of the CER into the stratum corneum was investigated *in vitro* using a multi-layer membrane model.

Results The MEs exhibited excellent thermodynamic stability (>2 years) and loading capacity (0.5% CER [AP]). The pseudo-ternary phase diagrams of the MEs were obtained and PCS results showed that the droplets are spherical in shape and bigger in size. *In vitro* investigations showed that the MEs exhibited excellent rate and extent of release and penetration.

Conclusions Stable lecithin-based CER [AP] MEs that significantly enhance the solubility and penetration of CER [AP] into the stratum corneum were developed. The MEs also have better properties than the previously reported polyglycerol fatty acid surfactant-based CER [AP] MEs.

KEY WORDS ceramide [AP] · lecithin · microemulsions · release and penetration · stratum corneum

ABBREVIATIONS

ABC	area between the curves
a_N	hyperfine splitting constant/isotropic hyperfine coupling constant
AUC	area under the curve
BC	bicontinuous
CER [AP]	Ceramide AP
Co-SAA	co-surfactant
DMSO	dimethyl sulfoxide
DSC	differential scanning calorimetry
EPR	electron paramagnetic resonance
HD-PMI	14 N HD-PMI (2-heptadecyl-2, 3, 4, 5, 5-pentamethyl-imidazoline-1-oxyl)
IF	line shape factor
LC	liquid crystalline
LW	line width factor
MDT	mean dissolution time
ME	microemulsion
Miglyol	Miglyol® 812
M_o	total percentage of dose released and penetrated
PCS	photon correlation spectroscopy
PeG	1, 2 pentandiol

F. F. Sahle · H. Metz · R. H. H. Neubert
Dept. of Pharmaceutical Technology & Biopharmaceutics
Institute of Pharmacy
Martin Luther University Halle-Wittenberg
Halle (Saale), Germany

J. Wohlrab
Department of Dermatology and Venereology
Medical Faculty
Martin Luther University Halle-Wittenberg
Halle (Saale), Germany

R. H. H. Neubert (✉)
Department of Pharmaceutical Technology and Biopharmaceutics
Martin Luther University Halle-Wittenberg
Wolfgang-Langenbeck Str. 4
06120 Halle (Saale), Germany
e-mail: reinhard.neubert@pharmazie.uni-halle.de

Present Address:
F. F. Sahle
Department of Pharmaceutics and Social Pharmacy, School of Pharmacy
College of Health Sciences, Addis Ababa University
Addis Ababa, Ethiopia

Phosal	Phosal® 75 SA
SAA	surfactant (surface active agent)
τ_c	rotational correlation time

INTRODUCTION

The stratum corneum contains about 15 layers of corneocytes embedded in a stratum corneum lipid matrix: a complex lipid mixture that is organised uniquely into a highly ordered multilamellar lipid sheets (1,2), which form the only continuous, tortuous path across the stratum corneum (2,3). The barrier function of the skin primarily lies on these lipid sheets, which are formed mainly from CERs, free fatty acids and cholesterol (4). Maintaining the right proportion and organisation of these lipids in the lipid matrix is of paramount importance for the skin to retain its barrier function. Any disturbance to the stratum corneum lipid composition might lead to altered and porous stratum corneum lipid lamellae (5,6) that allow the passage of exogenous substances into the stratum corneum. This, in turn, could induce inflammatory reactions that further result in perturbation of the barrier function, potentially establishing a vicious cycle that may severely damage the skin barrier (4). Conversely, studies have shown that several skin diseases such as psoriasis (7), atopic dermatitis and irritant/allergic contact dermatitis (8) are associated with depletion or disturbance of stratum corneum lipids.

CERs are sphingolipid metabolites that contain a sphingoid moiety (which can be sphingosine (S), dihydrosphingosine (D), phytosphingosine (P) or 6-hydroxy-sphingosine (H)) joined with a long chain free fatty acid moiety (which can be nonhydroxy (N), α-hydroxy (A), or ester-linked ω-hydroxy (EO)) through an amide bond (9). The different combinations of these sphingoid and free fatty acid moieties give rise to 12 different classes of CERs, which all have been identified in human stratum corneum (10). Owing to their inherent nature, CERs play a major role in the water-retaining properties of the epidermis and are claimed to dramatically increase skin's hydration level, repair the cutaneous barrier, prevent vital moisture loss, and contribute to reducing dry flaky skin and aged appearance (11). They can also be used against some skin diseases such as atopic dermatitis (11) and psoriasis (9) and in some other skin conditions like erythema, pruritus, and fissuring (12). Apart from their structural role, CERs also play an important role in intracellular signalling and regulation of several biological processes, such as proliferation, differentiation, apoptosis, inflammation and immune responses (13).

Schröter *et al.* (2009) reported that CER [AP], a short-chain CER containing a phytosphingosine moiety attached with α-hydroxy free fatty acid induces the formation of superstable lamellae (14). CER [AP] has also been shown to have some antiproliferative and proapoptotic activities in numerous cancer cell types *in vitro* (15). Hence, CERs, like CER [AP], have drawn attention as active compounds in both pharmaceutical and cosmetic industries (11). However, these lipids, to be mingled into the stratum corneum, should cross the stratum corneum and reach the stratum corneum-stratum granulosum interface, where the lipids are arranged into meaningful lamellae (1,16). Alternatively, they should penetrate into the deeper layers of the epidermis, whereby the uptake of lipids by nucleated epidermal cell layers takes place followed by release of the lipid mixture into nascent lamellar bilayers in the stratum corneum interstices (12). Nonetheless, the effectiveness of these lipids is limited due to their inherent hydrophobicity and potential precipitation as fine lipid suspensions when administered in hydrophilic formulations. Moreover, from conventional dosage forms, they cannot penetrate the stratum corneum to reach the site where they exert their biological activity (15,17). Thus, their administration demands designing of appropriate dosage forms, like MEs, that can enhance their solubility and permeation into the stratum corneum to a greater degree.

MEs are transparent, low viscous, optically isotropic and thermodynamically stable colloidal dispersions of oil and water, which are stabilised by an interfacial film of a surfactant (SAA), in most cases in combination with a co-surfactant (co-SAA) (18,19). In comparison to many other colloidal systems they possess large solubilisation capacity, associated with their immense interfacial area and availability of various microdomains of different polarity within the same single-phase system (20). They can also tremendously enhance permeability of actives into and through biological membranes (21): the small droplets have increased chance of adhering to biomembranes and to transport bioactive molecules in a more controlled fashion (22).

In recent years, MEs have emerged as promising vehicles for dermal and transdermal delivery of drugs (21,23). This might be attributed to the interaction of their components with the stratum corneum to reduce its diffusion barrier, their ability to increase concentration and thermodynamic activity of drugs at the site of application, and their hydration effect on the stratum corneum (23). To this effect, Sahle *et al.* (24) have developed polyglycerol fatty acid ester SAA-based MEs for the delivery of CER [AP] into the stratum corneum. However, the MEs developed were bigger in size and non spherical in shape. Therefore, the objective of this work was to develop CER [AP] MEs with better stability, loading capacity and other characteristics, based on another safe but natural SAA, lecithin.

MATERIALS AND METHODS

Materials

CER [AP] was generously donated by Evonik-Goldschmidt GmbH, Essen, Germany. PeG was a gift from Symrise

GmbH & Co KG, Holzminden, Germany. Miglyol and 4% collodion were purchased from Caesar & Loretz GmbH, Hilden, Germany. Phosal® 75 SA (phosal) was kindly donated by Phospholipid GmbH, Köln, Germany. 14 N HD-PMI (2-heptadecyl-2, 3, 4, 5, 5-pentamethyl-imidazoline-1-oxyl: HD-PMI) was obtained from the Institute of Chemical Kinetics and Combustion, Novosibirsk, Russia. Acetic acid was bought from Grüssing GmbH, Filsum, Germany. n-hexane and chloroform were procured from NeoLab Migge GmbH, Heidlberg, Germany and Merck, Darmstadt, Germany, respectively. Diethyl ether and HPLC grade methanol were purchased from Overlake GmbH, Leipzig, Germany and VWR international, Darmstadt, Germany, respectively. Absolute ethanol was supplied by the Bundesmonopolverwaltung für Branntwein, Offenbach, Germany. Non-ionic emulsifying alcohol and glycerol (85%) were obtained from Bombastus-Werke AG, Freital, Germany. Liquid paraffin was obtained from Hansen & Rosenthal KG, Hamburg, Germany. Dimethyl sulfoxide (DMSO) and anhydrous citric acid were bought from Carl Roth GmbH, Karlsruhe, Germany. Potassium sorbate was supplied by Fluka, Buchs, Switzerland. Octanol and dodecanol were obtained from Sasol Germany GmbH, Brunsbüttel, Germany. Double distilled water was used throughout the experiment.

Methods

Preparation of MEs

Since CER [AP] was poorly soluble in all the ingredients used for ME preparation, during ME preparation, the ME mixture was sonicated for about 1 h at 50°C. Alternatively, the MEs could be prepared at 80°C without sonication in less than 5 min.

Construction of Pseudo-Ternary Phase Diagram

Pseudo-ternary phase diagrams were constructed at room temperature through titration of 2 g of oil-SAA mixtures (10:90, 20:80, 30:70, 40:60, 50:50, 60:40, 70:30, 80:20 and 90:10, w/w) using increasing amount of 10 µl of the hydrophilic phase. Appearance of turbidity was taken as end point detector.

Cross-Polarised Light Microscopy

Determination of the isotropic nature of the MEs was conducted using a cross-polarised light microscope (Zeiss Axiolab Pol, Carl Zeiss MicroImaging GmbH, Jena, Germany). The same method was also employed to observe hazy systems within the pseudo-ternary phase diagram to identify whether they are stable emulsions or LC phases.

Electrical Conductivity

The electrical conductivity of the MEs, as a function of percent hydrophilic phase, was measured at 25 ± 0.2°C using a conductivity meter (Cyberscan con 11 conductivity/TDS/°C meter, EUTECH Instruments, Singapore) at various SAA-oil dilution lines. Following each addition of the hydrophilic phase, the system was subjected to magnetic stirring for about 1 min and was allowed until the temperature equilibrated and the conductivity readings stabilized. Conductivity readings were carried out in triplicates and the average and SD were calculated.

Differential Scanning Calorimetry

The DSC thermogram of MEs was obtained from −60 to 25°C using a DSC (DSC 200, Netzsch-Gerätebau GmbH, Selb, Germany), which was equipped with an automatic liquid N_2 cooling unit. Prior to DSC measurements, about 10 mg of the sample was filled in an aluminium pan and was pressure sealed. Another empty pressure sealed aluminium pan was also used as a reference. During the experiment the temperature was increased at a rate of $5°C\,min^{-1}$ and N_2 gas was used as a purging gas, at a flow rate of 10 ml/min.

Refractive Index

The refractive indexes of selected stable MEs were obtained using an Abbe refractometer (Carl-Zeiss, Jena, Germany) at 25 ± 2°C. The readings were made in triplicate and the average and the RSD were calculated.

Viscosity

The viscosity of selected MEs was measured at 25 ± 0.2°C, at 16 different shear rates ($0.1–100\ s^{-1}$) by using a rotational viscometer (Anton Paar GmbH, Graz, Austria). Since all the MEs exhibited Newtonian flow, the average of the viscosity results and RSD values were obtained.

Dynamic Light Scattering

Determination of MEs diameter was conducted at 25°C using a PCS hardware setup (ALV-Laser, Langen, Germany). A green Nd: YAG DPSS-200 laser (532 nm, Coherent, Auburn, USA) with an output of 200 mW was used as a light source. The sample cell was placed on a motor-driven precision goniometer (± 0.01°), which allows the photomultiplier detector to rotate from 20° to 150° scattering angles, and was allowed to stand for 10 min to equilibrate the temperature. The second order intensity time correlation functions (g^2) was recorded with an ALV-5000E Multiple Tau Digital Correlator (ALV-Laser Vertriebsgesellschaft

M-B.H., Langen, Germany) with fast option, with a sampling time of 60 s. Cylindrical sample cells made of Suprasil® quartz glass (10 mmdm: Hellma, Mühlheim, Germany) were used as sample holders. The measurements were conducted at different angles (30, 50, 70, 90, 110 and 130°) and the results were analysed employing appropriate equations and principles.

Electron Paramagnetic Resonance (EPR)

EPR spectra were recorded at constant temperatures using a Miniscope MS 200 X-Band spectrometer (Magnettech Berlin, Germany) operating at X band (9.4 GHz). Pyrex capillary tubes (~0.5 mm internal dm) were used as sample holders and the sample temperature was controlled using N_2 gas flow through the dewar vessel (± 0.1°C). The spectra were recorded for 24 h after sample preparation. HD-PMI was used as a spin probe at a concentration of 0.5 mM. The EPR setup include modulation amplitude of 0.02 mT, microwave frequency of 9.4 GHz/microwave power of 20 mW, centre magnetic field of 334.9 mT, sweep width of 4.95 mT and time constant of 40.96 ms. Fitting of the ESR spectra was performed using a Nitroxide spectra simulation software V. 4.99 (Biophysical laboratory EPR centre, Josef Stefan Institute, Ljubljana, Slovenia) and the rotational correlation time ($_c$), hyperfine splitting constant/isotropic hyperfine coupling constant (a_N), the line shape factor (IF) and the line width factor (LW) were determined and the results were analysed.

Assessment of Thermodynamic Stability

The physical stability of the MEs was routinely determined at ambient conditions, through visual inspection of the samples over 2 years. The MEs were also challenged through centrifugation (MLW T62, VEB MLW Medizintechnik, Leipzig, Germany) at 3,500 rpm for 30 min after 1 week of preparation. Physical changes, such as, turbidity, phase separation, flocculation of ME droplets and/or precipitation of the dispersed lipid were taken as indicators of physical instability.

Preparation of Model Membrane

Preparation of a model membrane was preceded by preparation of a 100 g membrane solution, which contains 50 g 4% (m/m) collodion solution and 50 g 8% (m/m) dodecanol mixture (dodecanol-octanol-DMSO, 80:10:10, v/v/v) in ethanol-diethyl ether, 1.5:8.5, v/v. Membrane films were prepared by evenly spreading the membrane solution over a glass surface of about (500 mm × 300 mm), which was mounted on a film applicator with adjustable clearance (Workshop, Institute of Pharmacy, Martin Luther University Halle-Wittenberg), and allowing the solvent to slowly evaporate under a fume hood for about 12 h. Finally, the film was carefully removed from the surface of the film applicator and was cut into 40 mm diameter discs before fitting it into a multi-layer membrane model apparatus.

In Vitro Release and Penetration Study

The rate and extent of release and penetration of CER [AP] from various dosage forms was investigated *in-vitro* using a multi-layer membrane model described by Neubert *et al.* (1991) (25). Briefly describing the model, it contains penetration cells arranged one over the other on a penetration cell stand. Each penetration cell had a circular base plate, on which a stencil and an upper cover plate were put. Four layers of the 40 mm membrane discs were arranged one over the other and were sandwiched in-between the circular base plate and the stencil. To prevent adhesion of the bottom membrane to the base plate, a nitrocellulose film was put between the bottom membrane and the circular base plate. The stencil had 4 cm^2 square opening at the centre, through which the formulations were applied. In our case an equivalent mass of the formulation that contain 50 µg CER [AP] was evenly spread through the stencil over the upper membrane and the cells were kept at 32°C in a thermostatic chamber for predetermined time intervals (15, 30, 60,120 and 180 min), allowing release and penetration of CER [AP]. Then the formulation remained unabsorbed on the surface of the first layer was removed using a tissue paper (except those cells used to calculate the percentage recovery), and the amount of CER [AP] released and penetrated into each layer was extracted through sonication of the membranes in 1 ml n-Hexane-ethanol (2:1, v/v) at 50°C for 30 min. The amount of CER [AP] extracted was, finally, quantified using AMD-HPTLC. During the experiment five test and three recovery replicates were studied. To investigate any possible interaction of the formulation components with CER [AP] peak, blank experiment was also conducted at 180 min. One-way ANOVA ($p < 0.05$), followed by Tukey's test as post hoc analysis, was used to indicate the existence of significant differences between sets of data.

Automated Multiple Development (AMD)-HPTLC

Quantification of CER [AP] was conducted by a Camag HPTLC with a CAMAG win CATS planer chromatographic manager (Camag, Muttenz, Switzerland). During the experiment, 5 µl of the test and standard samples were applied as 3 mm bands at 6 mm intervals, under N_2 stream on a TLC plate (TLC silica gel 60 F254, 20 cm × 10 cm, Merck KGaA, Darmstadt, Germany) using CAMAG Automatic TLC sampler 4. Chromatographic developments were conducted twice in CAMAG AMD 2 using chloroform-methanol-acetic acid (94.5:5:0.5, v/v/v) as a mobile phase over a distance of

70 mm. After chromatographic development, the HPTLC plate was dipped in an aqueous CuSO4 solution (10% CuSO4 (w/v), 8% phosphoric acid (w/v) and 5% methanol (v/v)) for 20 s. and was charred in an oven for 20 min, at 160° C. Finally, the plate was scanned by a CAMAG TLC Scanner 3 in absorbance mode (358 nm) and the results were analyzed.

RESULTS

Formulation of Lecithin-Based CER [AP] MEs

Stable lecithin based CER [AP] MEs were formulated and optimised using phosal, miglyol and water-PeG mixture as amphiphilic, oil and hydrophilic components, respectively. The obtained stable ME regions are shown in Fig. 1d–f and ten stable MEs from these regions were selected for further characterization (Table I). As can be seen in the figures and table, the stability and loading capacity of the MEs increased as the percentage of water in the hydrophilic phase decreased.

Construction of Pseudo-Ternary Phase Diagrams

The pseudo-ternary phase diagrams of the MEs constructed using titration techniques is shown in Fig. 1. The LC regions that exhibited birefringence when examined under a cross-polarised light microscope are also depicted.

Electrical Conductivity

As has been depicted in Fig. 2, the electrical conductivity of lecithin-based MEs, obtained at various dilution lines for various ME systems, exhibited abrupt changes, which was attributed to the change in ME nanostructure.

Differential Scanning Calorimetry

The DSC thermograms of lecithin based MEs were obtained at 40% SAA dilution line using water-PeG (3.5:6.5, v/v) as a titrating phase (Fig. 3). As can be seen in the figure, the oil peak appeared at around −5°C, which was moved to lower temperatures until it vanished at 50% of the hydrophilic component. In addition, an exothermic peak was obtained at lower temperatures (≈ −48°C) for MEs containing 35 to 45% of the hydrophilic component.

Electron Paramagnetic Resonance

The plot of the four EPR parameters, τ_c, IF, LW and a_N, as a function of percent hydrophilic component, which were obtained on the 40% SAA dilution line, at 25°C and 40°C are shown in Fig. 4. The results in the figure showed abrupt changes in the EPR parameters along the dilution line as a function of wt % of the hydrophilic phase, which is associated with changes in ME nanostructure.

Viscosity, Refractive Index and Droplet Size

The viscosity, refractive index, droplet diameter and the nanostructures of the 10 optimized lecithin-based CER [AP] MEs (Table I) are given in Table II. The results showed that, those MEs with higher percentage of the SAA exhibited higher viscosities and, generally, the MEs have relatively bigger droplet sizes.

Micropolarity and Microviscosity

The micropolarity and microviscosity of selected lecithin-based CER [AP] MEs, determined using EPR technique and HD-PMI as a spin probe (24), are shown in Table III. In addition, as has been depicted in Fig. 5, ME microviscosity decreases logarithmically as the temperature increased.

In Vitro Release and Penetration Study

Figure 6 a–c depict the release and penetration of CER [AP] from selected lecithin based CER [AP] MEs. During the study a hydrophilic cream (DAC) containing 0.5% CER [AP] was used as a reference formulation. As can be seen in the figures, within 15 min, a higher percentage of CER [AP] was released from the MEs and penetrated into deeper membrane layers unlike the hydrophilic cream which was released to a lesser extent and penetrated only to the second membrane.

In addition, the total amount of CER [AP] released and penetrated as a function of time into the four membrane layers is shown in Fig. 7. Moreover, the key *in vitro* pharmacokinetic parameters describing the rate and extent of release and penetration process, which include area under the curve (AUC), area between the curves (ABC); total percent CER [AP] released and penetrated (M_o) and mean dissolution time (MDT) were obtained (Table IV). As can clearly be seen in the figure and the table, the rate and extent of release and penetration of CER [AP] from the MEs was by far better than the conventional hydrophilic cream. Nonetheless, the difference in the rate and extent of CER [AP] released and penetrated from PAPOME2 and PAPOME8 was statistically insignificant ($P<0.05$).

DISCUSSION

Formulation of Stable Lecithin-Based CER [AP] MEs

Although there are some conventional preparations containing CERs in the market (e.g. TriCeram, Atopiclair and Mimyx Cream), it was reported that larger and extremely lipophilic molecules like CERs can hardly permeate the skin from such

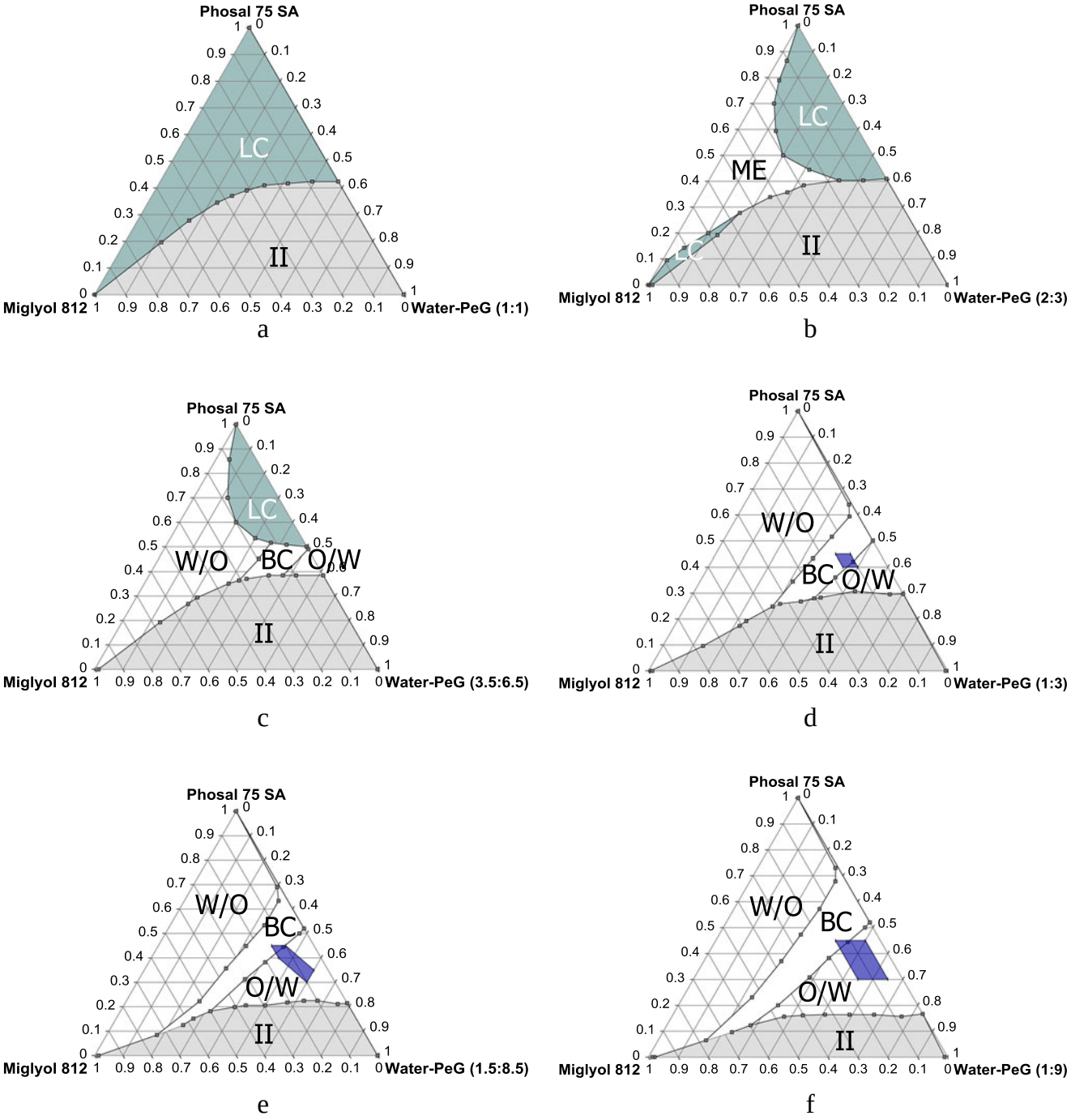

Fig. 1 Pseudo-ternary phase diagrams of lecithin-based MEs at different water-PeG ratios: (**a**) 1:1; (**b**) 2:3; (**c**) 3.5:6.5; (**d**) 1:3; (**e**) 1.5:8.5 and (**f**) 1:9. II= 2 phase region; ME= ME region; O/W= O/W ME region; W/O= W/O ME region; BC= bicontinuous (BC) ME region; LC= LC ME region, the dark band on the ME region=region of stable CER [AP] MEs.

dosage forms. Thus, to effect the penetration of CER [AP] deep into the stratum corneum-stratum granulosum interface or the upper layers of the epidermis, we had developed polyglycerol fatty acid ester SAA-based MEs (24). However, the MEs were formulated using synthetic SAAs and the obtained droplets were irregular in shape and bigger in size, which might affect their penetration into the target site. Hence, other class of CER [AP] MEs that are spherical in shape, smaller in size and with superior stability and loading capacity were developed using the biological and safe SAA, lecithin. These classes of MEs were referred as lecithin-based CER [AP] MEs.

During the development of lecithin based CER [AP] MEs, various oils and co-solvents were screened and the most stable lecithin-based CER [AP] MEs were obtained

Table I Compositions and Stabilities of Optimised Lecithin-Based CER [AP] MEs

No.	ME	Miglyol %	Phosal %	Water-PeG (1:9) %	Water-PeG (1.5:8.5) %	Water-PeG (1:3) %	CER [AP][a] %	Stability (SD) (Mon)
1	PAPOME1	10	40	–	–	50	0.3	> 24
2	PAPOME2	10	45	–	–	45	0.3	> 24
3	PAPOME3	5	35	–	60	–	0.5	> 24
4	PAPOME4	10	45	–	45	–	0.5	> 24
5	PAPOME5	15	45	–	40	–	0.5	16 (1)
6	PAPOME6	10	30	60	–	–	0.5	15 (1)
7	PAPOME7	15	35	50	–	–	0.5	> 24
8	PAPOME8	10	40	50	–	–	0.5	> 24
9	PAPOME9	5	35	60	–	–	0.5	> 24
10	PAPOME10	15	45	40	–	–	0.5	> 24

[a] percent per total mass of the MEs

using miglyol and water-PeG mixture as oil and hydrophilic components, respectively. In addition, the effect of the percentage of each ME component on the stability of the MEs was assessed in order to obtain MEs with optimum characterstics (Fig. 1d–f). During optimization, the levels of the oil and SAA components were maintained at 5–15% and ≤45%, in order to insure formation of O/W MEs and safety, respectively. As can be seen in Fig. 1d–f and Table I, the stability and loading capacity of the MEs increased as the percentage of water in the hydrophilic phase decreased, which can highly be attributed to the hydrophobic nature of the lipid.

Characterization of Lecithin-Based CER [AP] MEs

Construction of Pseudo-Ternary Phase Diagrams

During construction of the pseudo-ternary phase diagrams, Fig. 1, titration technique was employed to separate one phase and two phase regions. The clear single phase region

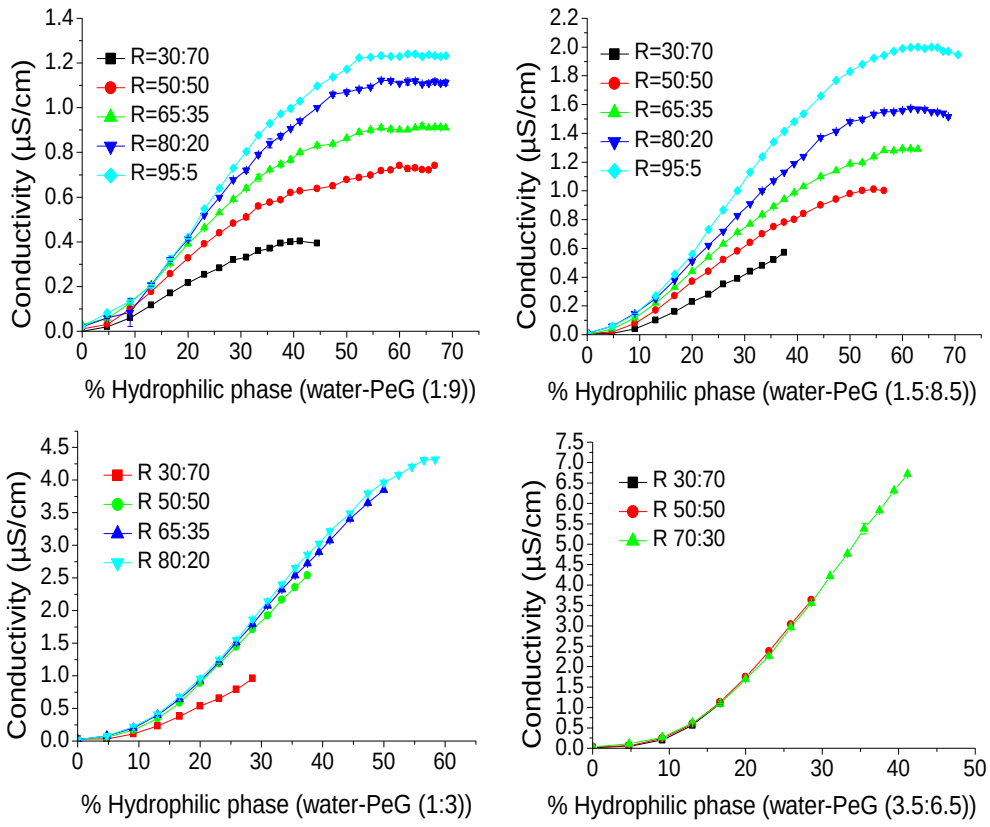

Fig. 2 Electrical conductivity of lecithin-based MEs as a function of wt% of the hydrophilic phase (water-PeG 1:9 to 3.5:6.5). R= phosal-miglyol (% m/m) (*N*=3).

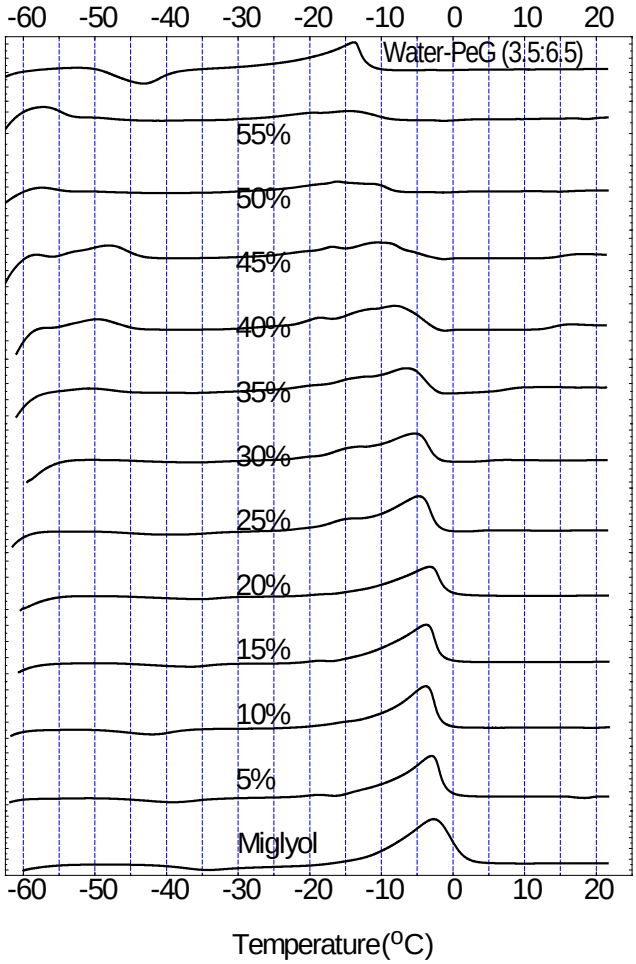

Fig. 3 The DSC thermograms of lecithin-based MEs obtained along the 40% SAA dilution line at various wt% of the hydrophilic phase (water-PeG 3.5:6.5).

was further examined under a cross-polarised light microscope and those systems that exhibited birefringence were classified as LCs (26–28).

As can be seen in the figure, at water-PeG (1:1, v/v) only LCs were obtained, which most likely represents a lamellar liquid crystalline phase formed due to less amount of the co-solvent that provides the desired flexibility for the interfacial film to form MEs (29). It was also shown that lecithin, unlike most twin tailed SAAs, cannot form MEs on its own without addition of a co-SAA or a co-solvent, which disrupts lamellar structures that they form (30). Moreover, studies have shown that, unlike alcohols, alkanediols need to be used at high concentrations in order to obtain stable MEs (31). Thus, the two-phase and LC regions contracted tremendously as the percentage of PeG in the hydrophilic phase increases and at water-PeG≤1:3 the LC region vanished completely.

Determination of ME Nanostructure

Since, in most cases, determination of ME nanostructures needs the use of combination of different techniques, the nanostructures of lecithin-based CER [AP] MEs were determined using electrical conductivity experiments in combination with DSC and EPR techniques.

Electrical conductivity is the simplest and most important technique by which valuable information regarding MEs nanostructure is obtained. Hence, the electrical conductivity of lecithin-based MEs was obtained at various dilution lines for various ME systems, Fig. 2. As can be seen in the figure, initially the electrical conductivity was zero followed by a slow increase, which can be attributed to percolation of hydrophilic droplets into clusters (32). Then an abrupt increase in electrical conductivity was observed that could arise through formation of channels of the hydrophilic component, which is a characteristic of BC MEs. Finally, the electrical conductivity increased slowly, suggesting formation of O/W MEs. Accordingly, the W/O, BC and O/W ME regions for most of the pseudo-ternary phase diagrams were obtained (Fig. 1).

Corroborating the electrical conductivity experiments, in the DSC thermograms of the MEs (Fig. 3), the oil peak moved to lower temperatures as the percentage of hydrophilic phase increases and finally vanished at 50% of the hydrophilic component. The exothermic peak obtained at lower temperatures (≈ −48°C) for MEs containing 35 to 45% of the hydrophilic component, was also attributed to the bound water to the head group of the SAA. Same DSC peaks, representing BC MEs, were observed by Hathout *et al.* (2010) (27) and Sahle *et al.* (24). However, due to the low percentage of water in the hydrophilic phase, strong unbound water peaks of the O/W MEs were not seen. Hence, the results obtained suggest that the MEs are 0–35% W/O, 40–45% BC and above 50% O/W types, at the 40% SAA dilution line, where the result is in agreement with that of electrical conductivity results.

Moreover, the results of EPR experiments, as has been discussed in detail in our previous work (24), was used to supplement the results of conductivity and DSC results. In this experiment, the same principle applied in (24) was used to analyse the plot of the four EPR parameters, τ_c, IF, LW and a_N, as a function of percent hydrophilic component, which were obtained on the 40% SAA dilution line, at 25°C and 40°C (Fig. 4). Thus, the abrupt changes in the EPR parameters along the dilution line as a function of wt % of the hydrophilic phase were associated with changes in ME nanostructure. Accordingly, at 25°C, a system with 0–30% of the hydrophilic phase (water-PeG 1.5:8.5 w/w) was classified as W/O ME, 35–40% was classified as BC ME and above 45% the region was classified as O/W ME region. However, as the ratio of PeG in the hydrophilic phase decreases (water-PeG 3.5:6.5) the BC region moved to

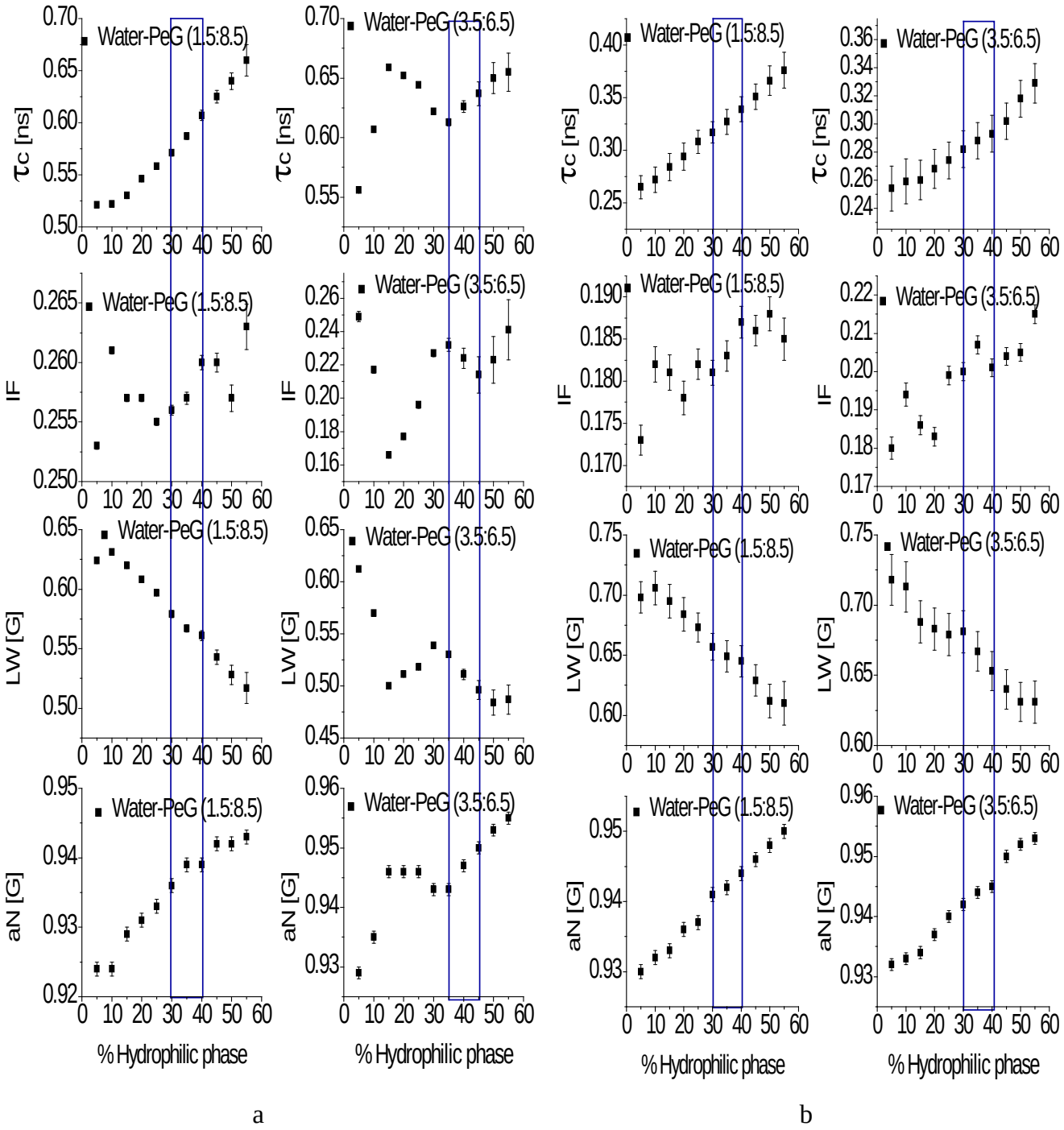

Fig. 4 Change in EPR parameters of lecithin-based MEs at 40% SAA dilution line at 25°C (**a**) and 40°C (**b**) as a function of percentage water-PeG (1.5:8.5, v/v) (*left*) and (1:1, v/v) (*right*).

40–45% of the hydrophilic phase, by expanding the W/O ME region to 0–35% and contracting the O/W ME region to >50%. Besides, as can be seen in the figure, the increase in temperature did not significantly affect the MEs nanostructure, except in those MEs obtained using water-PeG 3.5:6.5 w/w, where the different ME regions shifted slightly to the left. This, however, can justify the slight shift of the BC region towards the right in the case of DSC results. The EPR results obtained are also in agreement with the results of conductivity and DSC experiments. Therefore, the different regions of ME nanostructures were revealed using a combination of electrical conductivity, DSC and EPR results as has been depicted in Fig. 1c–f.

Table II Viscosity, Refractive Index, Droplet Diameter and Nanostructure of the Optimised Lecithin-Based CER [AP] MEs

No.	ME	Viscosity (RSD)[a] (mPa.s)	Refractive index (RSD)	Droplet diameter (RSD) (nm)	Nanostructure
1	PAPOME1	52.3 (0.57)	1.442 (0.042)	204.2 (5.9)	O/W
2	PAPOME2	60.3 (1.23)	1.441 (0.042)	176.9 (7.5)	O/W
3	PAPOME3	49.6 (0.99)	1.440 (0.042)	194.7 (22.9)	O/W
4	PAPOME4	66.6 (0.98)	1.440 (0.000)	163.4 (12.2)	O/W
5	PAPOME5	66.4 (0.48)	1.442 (0.069)	214.6 (7.5)	O/W
6	PAPOME6	45.7 (0.24)	1.446 (0.042)	223.2 (7.0)	O/W
7	PAPOME7	58.6 (1.13)	1.441 (0.042)	167.9 (5.7)	O/W
8	PAPOME8	61.4 (1.73)	1.442 (0.042)	197.1 (5.5)	O/W
9	PAPOME9	52.6 (0.26)	1.440 (0.083)	196.9 (6.4)	O/W
10	PAPOME10	59.2 (0.79)	1.442 (0.042)	1848.8 (69.7)	BC

[a]exhibited Newtonian type of flow

Determination of ME Viscosity, Refractive Index and Droplet Size

As has been shown in Table II, all the formulations had relatively low viscosity and underwent Newtonian type of flow, which is typical characteristic of MEs (33).

Since the results of electrical conductivity, DSC and EPR data showed change in nanostructure upon dilution of the MEs, measurement of droplets diameter was carried out without diluting the MEs. During the measurement, the second order intensity autocorrelation function of the MEs (g^2 (q; τ): q is wave vector (momentum transfer) and τ is delay time) was obtained at various angles (30, 50, 70, 90, 110, 130°) and the first order (field) autocorrelation function (g^1 (q; τ)) was calculated using Siegert Eqn., Eq. 1 (34,35).

$$g2(q;\tau) = 1 + \beta|g1(q;\tau)|^2 \quad (1)$$

where; β is the coherence factor of the experiment.

Assuming a mono-dispersed population, g^1 (q; τ) can be treated as a single exponential decay, Eq. 2 (36).

$$g1(q;\tau) = \exp^{\uparrow}((-\Gamma\tau)) \quad (2)$$

where Γ is the decay rate.

The g^1 (q; τ) *vs.* τ curve fitting was made to determine the decay half time ($t_{1/2}$) and Γ was calculated as $1/(t_{1/2})$.

Table III Relative a_N Values, Microviscosities and Viscosities of Selected Lecithin-Based MEs at 25°C Along with their Proposed Nanostructures

No.	ME[a]	a_N	Microviscosity (mPa.s)	Viscosity (RSD) (mPa.s)	Nanostructure
1	PAPOME2	0.945	24.22	60.3 (1.227)	BC
2	PAPOME8	0.940	34.55	61.4 (1.726)	O/W

[a] MEs were prepared without addition of CER [AP]

The apparent diffusion coefficient of the droplets was then calculated at a given angle using Eq. 3 (35).

$$\Gamma = q^2 D \quad (3)$$

where, q is the absolute value of the scattering vector and is given by Eq. 4 (37):

$$q = \frac{4\pi n}{\lambda} sin\left(\frac{\theta}{2}\right) \quad (4)$$

where, λ is the incident laser wavelength, n is the refractive index of the sample and θ is angle at which the detector is located with respect to the sample cell.

Then, the droplet diameter was calculated using Stokes-Einstein Eqn., Eq. 5 (35,38).

$$D = \frac{K_B T}{6\pi\eta r} \quad (5)$$

where K_B is Boltzmann's constant, T is the absolute temperature, η is viscosity of the medium and r is the radius of the droplet.

The results obtained showed that there was no significant difference observed between the apparent diffusion coefficient of the droplets obtained at various angles, suggesting that the dispersed droplets are spherical in shape (24,37). However, in PAPOME10, the apparent diffusion coefficient of the droplets values were angle dependent and Γ/q^2 *vs.* q^2 was non linear, suggesting that it is a BC type ME (24). It was shown that BC MEs can scatter light due to the dynamics and structural alterations of the BC channels (24). The nanostructures suggested by the PCS results were in line with the nanostructures depicted on the pseudo-ternary phase diagram, Fig. 1, except in case of PAPOME2 and 5, which were identified as BC type MEs. This shift in nanostructure can be attributed to the incorporation of CER [AP], which possibly altered the nanostructure of the MEs at the BC-O/W boarder owing to its amphiphilic nature. Thus, as was also supported by our previous work (24), apart

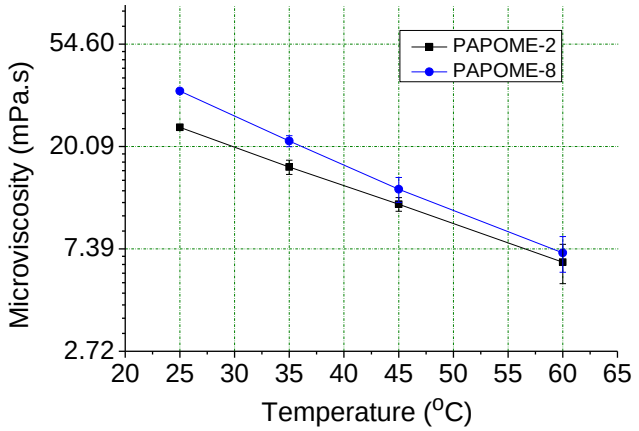

Fig. 5 Effect of temperature on microviscosity of selected lecithin-based MEs.

from measuring droplet size, PCS results can also be used as a means of identifying MEs nanostructures.

As can be seen in Table II, the hydrodynamic radius of the MEs is relatively bigger than the commonly reported MEs droplet diameter (10–100 nm (39,40)). However, stable MEs with bigger diameters were also previously reported (24,41,42). Besides, droplets of lecithin-based MEs containing higher concentration of the SAA and low level of oil were relatively smaller and similar results were obtained with lecithin based MEs (43,44).

Determination of ME Micropolarity and Microviscosity

Determination of ME micropolarity and microviscosity was carried out using EPR. During the measurement, a_N of the nitroxide free radicals (a parameter that is dependent on the polarity of the medium surrounding the spin probe, which affects the electron density around the N nuclei (45)) and τ_c were used as measures of micropolarity and microviscosity, respectively. In the absence of spin-spin interactions, an increase in τ_c indicates a decrease in the spin probe mobility, which is related to high microviscosity of the media surrounding the spin probe (46) and this relation can quantitatively be expressed by the modified Stokes-Einstein-Debye Eqn., Eq. 6 (47).

$$\tau_c = \left(\frac{\eta V}{K_B T}\right) k + \tau_o \qquad (6)$$

where k_B is Boltzmann's constant, T is absolute temperature, μ is viscosity of the medium, V is the molecular volume of the spin probe, and K is probe media interaction factor.

The absolute values of microviscosity can, therefore, be obtained following calibration of the ESR spectra of the spin probe in a solvent system with known viscosity (48), where in our case PeG (the co-solvent with known viscosities over a range of temperature (49) and is one of the major constituents of the ME) was used. Consequently, the τ_c (ns) *vs.* (η/T)

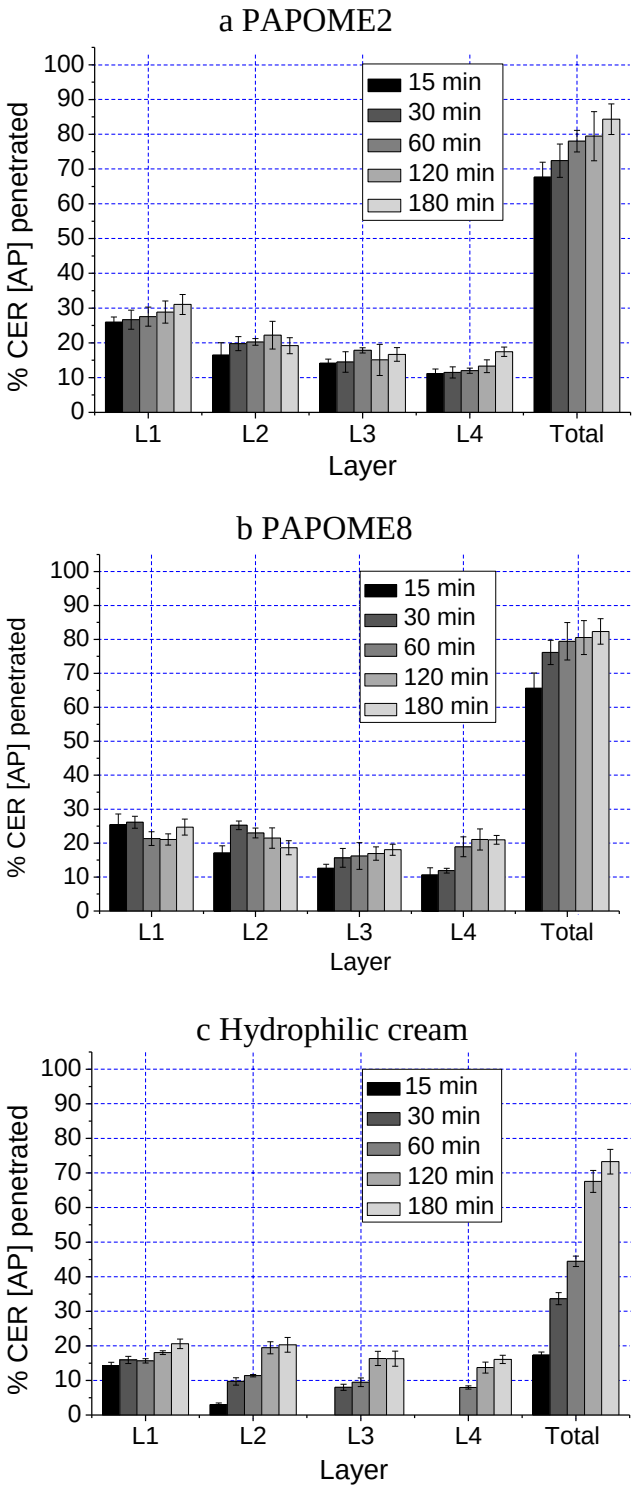

Fig. 6 Rate of CER [AP] released and penetrated into the four layers of the multi-layer membrane model ($N=5$) from various formulations.

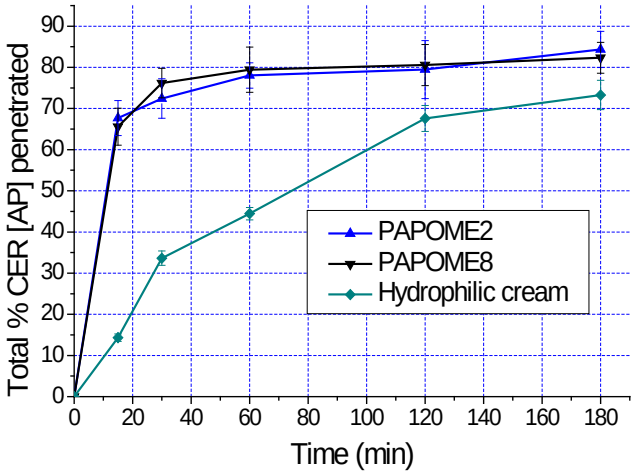

Fig. 7 Overall release and penetration profile of CER [AP] from various formulations into membranes of a multi-layer membrane model (*N*=5).

graph obtained was linear (R^2=0.9995), for $\tau_c \leq 1.2$ ns, and the equation describing the relationship between τ_c and η in PeG is given by Eq. 7.

$$\tau_c = 9.2907\left(\frac{\eta}{T}\right) + 0.0021 \quad (7)$$

Equation 7 can be used to obtain η values whenever HD-PMI is used as a spin probe, provided that the K value of the system (Eq. 6), that depends on the nature of the vehicle in which HD-PMI is dissolved, is determined. Hence, the K values (KV/K_B) in different vehicles with known viscosity (50) were calculated at specific temperatures, (Table V).

As can be seen in the table, given V and K_B are constants, the K values are different in different vehicles. The highest K was exhibited by PeG and the lowest by the miglyol. Thus, despite viscosity is not an additive behavior (50), for the purpose of estimation of the microviscosity of MEs, the average of the K values of miglyol and PeG was taken. This was done considering the fact that the lipophilic phase in which the spin probe is dissolved is formed mainly from miglyol-PeG mixture. Therefore, the equation that describes the relationship between τ_c and η was obtained, Eq. 8, and the micropolarity and microviscosity of the two selected lecithin-based CER [AP] MEs was calculated, Table III.

$$\tau_c = 7.41\left(\frac{\eta}{T}\right) + 0.0021 \quad (8)$$

a_N reflects the polarity of the immediate environment of the spin probe, irrespective of the degree of spin probe entrapment (51,52). PAPOME2 had higher micropolarity than PAPOME8 due to the higher percentage of water in the hydrophilic phase that, in turn, reduces the extent of partitioning of PeG into the oily phase. Although the higher SAA concentration in PAPOME2, which has more or less similar viscosity as that of PAPOME8, it has lower microviscosity than PAPOME8. The decrease in microviscosity can partially be attributed to the reduced partitioning of PeG into the oily phase. However, compared to alteration in a_N value, the decrease in microviscosity in PAPOME2 was quite significant and this can be accounted to the higher level of entrapment of the spin probe in the O/W droplets of PAPOME8 (51). The converse provides further information on the nanostructures of the MEs.

During investigation of the effect of temperature on ME microviscosity, the temperature was maintained above 25°C because bellow 5°C the MEs underwent anisotropic motion ($\tau_c > 3$ ns) (53,54) and the relationship between viscosity and τ_c remained linear for $\tau_c < 1.2$ ns, which was attained above 15°C.

Table V KV/K_B Values of HD-PMI Calculated in Selected ME Components

No.	Component	Temp (K)	Viscosity (mPa.s)	τ_c	$K.V/K_B$
2	miglyol	293.15	30.0	0.571	5.559
3	PeG	298.15	45.6	1.482	9.684
		303.15	33.5	1.034	9.337
		308.15	25.0	0.754	9.286
		313.15	18.8	0.554	9.188
4	H2O-PeG (1:9)	303.15	30.0	0.685	6.901
		293.15	55.0	1.332	7.088
		298.15	41.0	0.948	6.879
		308.15	24.0	0.507	6.483
		313.15	18.0	0.384	6.644
5	H2O-PeG (1:3)	303.15	25.6	0.459	5.411
6	H2O-PeG (1:1)	303.15	14.6	0.328	6.767

Table IV *In Vitro* Pharmacokinetic Parameters Obtained from Release and Penetration Study of CER [AP] from Selected Dosage Forms (*n*=5)

No.	Formulation	AUC (SD) (% . min)	M_o (SD) (%)	ABC (SD) (% . min)	MDT (SD) (min)
3	PAPOME2	13521 (183)	84.8 (2.8)	1745 (407)	20.4 (4.2)
4	PAPOME8	13592 (234)	82.8 (1.6)	1331 (361)	16.0 (4.1)
5	Hydrophilic cream	9185 (283)	73.3 (3.3)	4127 (561)	55.6 (5.5)

In Vitro Release and Penetration Study

The process of drug absorption through the skin involves liberation of actives from dosage forms, penetration through the stratum corneum, permeation through the epidermis and absorption into the blood vessels and lymphatic system. However, since the objective of this work was to strengthen

the barrier function of diseased, affected and/or aged skin by administering CER [AP] into the stratum corneum lipid lamella, particularly to the stratum corneum-stratum granulosum interface where integration of the CER into the lipid lamellae takes place, the primary focus was to investigate the release and penetration of the CER into the stratum corneum. Thus, the release and penetration of CER [AP] into the upper layers of the epidermis was investigated *in vitro* using a multi-layer membrane model described by Neubert *et al.* (25).

For the study a collodion-dodecanol membrane was chosen, where the collodion forms a mesh in which the dodecanol mixture was embedded in, simulating the stratum corneum lipid matrix by virtue of its lipophilicity (25). The dodecanol mixture (dodecanol-octanol-DMSO (8:1:1, v/v/v)) contained low percentages of octanol and DMSO to provide the membrane thermodynamic stability and to enhance the solubility of CER [AP] in the membrane, respectively. In addition, to maintain the sink condition four membranes were used during the experiment: where the membranes contain equivalent amount of the dodecanol mixture in which the maximum amount of CER [AP] dissolved remains below 15% of its saturation solubility, assuming 100% of the lipid is released and penetrated. The results of the study (Figs. 6a–c and 7) showed that release and penetration of the CER from the MEs is by far better than the hydrophilic cream.

Moreover, pharmaceutical formulations which exhibit lower MDT and higher AUC have better rate and extent of release and penetration, respectively. Hence the key *in vitro* pharmacokinetic parameters obtained (Table IV) showed that the MEs have tremendously improved the rate and extent of CER [AP] release and penetration in comparison to the hydrophilic cream. Therefore, release and penetration from MEs was much better than a conventional cream.

CONCLUSIONS

Stable lecithin based CER [AP] MEs were formulated and characterised. The pseudo-ternary phase diagrams designating the various phases as well as the nanostructures of MEs were also prepared. *In vitro* study showed that the MEs could tremendously improve the release and penetration of the CER in comparison to a hydrophilic cream. Compared to the previously developed polyglycerol fatty acid ester-based CER [AP] MEs (24), lecithin based CER [AP] MEs were smaller in size and spherical in shape, which may favour their penetration deep into the stratum corneum. They also have better stability, lipid loading capacity and other physicochemical characteristics than the previously developed MEs. Following toxicity and *in vivo* permeability investigation, these formulations may be of great significance in treating aged and affected skin.

ACKNOWLEDGMENTS AND DISCLOSURES

The authors would like to thank Manuela Woigk, Kerstin Schwarz and Adelheid Pötzsch for their excellent technical assistance. We are also grateful to Dr. Karsten Busse for his contribution in those experiments involving PCS. Fitsum F. Sahle greatly acknowledges the financial support provided by the German Academic Exchange Service (DAAD).

REFERENCES

1. Bonte F, Pinguet P, Saunois A, Meybeck A, Beugin S, Ollivon M, *et al.* Thermotropic phase behavior of *in vivo* extracted human stratum corneum lipids. Lipids. 1997;32(6):653–60.
2. Groen D, Gooris GS, Ponec M, Bouwstra JA. Two new methods for preparing a unique stratum corneum substitute. Biochim Biophys Acta. 2008;1778(10):2421–9.
3. de Jager MW, Gooris GS, Dolbnya IP, Ponec M, Bouwstra JA. Modelling the stratum corneum lipid organisation with synthetic lipid mixtures: the importance of synthetic ceramide composition. Biochim Biophys Acta. 2004;1664(2):132–40.
4. Loden M. The skin barrier and use of moisturizers in atopic dermatitis. Clin Dermatol. 2003;21(2):145–57.
5. Farwanah H, Neubert R, Zellmer S, Raith K. Improved procedure for the separation of major stratum corneum lipids by means of automated multiple development thin-layer chromatography. J Chromatogr B Anal Technol Biomed Life Sci. 2002;780(2):443–50.
6. Bonte F, Saunois A, Pinguet P, Meybeck A. Existence of a lipid gradient in the upper stratum corneum and its possible biological significance. Arch Dermatol Res. 1997;289(2):78–82.
7. Cho Y, Lew BL, Seong K, Kim NI. An inverse relationship between ceramide synthesis and clinical severity in patients with psoriasis. J Korean Med Sci. 2004;19(6):859–63.
8. Berardesca E, Barbareschi M, Veraldi S, Pimpinelli N. Evaluation of efficacy of a skin lipid mixture in patients with irritant contact dermatitis, allergic contact dermatitis or atopic dermatitis: a multicenter study. Contact Dermatitis. 2001;45(5):280–5.
9. Farwanah H, Raith K, Neubert RH, Wohlrab J. Ceramide profiles of the uninvolved skin in atopic dermatitis and psoriasis are comparable to those of healthy skin. Arch Dermatol Res. 2005;296(11):514–21.
10. van Smeden J, Hoppel L, van der Heijden R, Hankemeier T, Vreeken RJ, Bouwstra JA. LC/MS analysis of stratum corneum lipids: ceramide profiling and discovery. J Lipid Res. 2011;52(6):1211–21.
11. Zhang L, Hellgren LI, Xu X. Enzymatic production of ceramide from sphingomyelin. J Biotechnol. 2006;123(1):93–105.
12. Proksch E, Jensen JM, Elias PM. Skin lipids and epidermal differentiation in atopic dermatitis. Clin Dermatol. 2003;21(2):134–44.
13. Kang JS, Yoon WK, Youm JK, Jeong SK, Park BD, Han MH, *et al.* Inhibition of atopic dermatitis-like skin lesions by topical application of a novel ceramide derivative, K6PC-9p, in NC/Nga mice. Exp Dermatol. 2008;17(11):958–64.
14. Schroter A, Kessner D, Kiselev MA, Hauss T, Dante S, Neubert RH. Basic nanostructure of stratum corneum lipid matrices based on ceramides [EOS] and [AP]: a neutron diffraction study. Biophys J. 2009;97(4):1104–14.
15. Stover TC, Sharma A, Robertson GP, Kester M. Systemic delivery of liposomal short-chain ceramide limits solid tumor growth in murine models of breast adenocarcinoma. Clin Cancer Res. 2005;11(9):3465–74.

16. Weerheim A, Ponec M. Determination of stratum corneum lipid profile by tape stripping in combination with high-performance thin-layer chromatography. Arch Dermatol Res. 2001;293(4):191–9.
17. Lambers JWJ, Pijnacker NL, Verweij J, Leiden NL, inventors; Gist-brocades N.V. (NL), assignee. Ceramide 3 derivatives based on monounsaturated fatty acids. United States patent 5693677; 1997.
18. Boonme P, Krauel K, Graf A, Rades T, Junyaprasert VB. Characterization of microemulsion structures in the pseudoternary phase diagram of isopropyl palmitate/water/Brij 97:1-butanol. AAPS PharmSciTech. 2006;7(2):E45.
19. Xu J, Fan QJ, Yin ZQ, Li XT, Du YH, Jia RY, *et al.* The preparation of neem oil microemulsion (Azadirachta indica) and the comparison of acaricidal time between neem oil microemulsion and other formulations *in vitro*. Vet Parasitol. 2010;169(3–4):399–403.
20. Chaiyana W, Saeio K, Hennink WE, Okonogi S. Characterization of potent anticholinesterase plant oil based microemulsion. Int J Pharm. 2010;401(1–2):32–40.
21. Liu CH, Chang FY, Hung DK. Terpene microemulsions for transdermal curcumin delivery: effects of terpenes and cosurfactants. Colloids Surf B Biointerfaces. 2011;82(1):63–70.
22. Fanun M. Oil type effect on diclofenac solubilization in mixed nonionic surfactants microemulsions. Colloids Surf, A Physicochem Eng Asp. 2009;343(1–3):75–82.
23. Zhu W, Guo C, Yu A, Gao Y, Cao F, Zhai G. Microemulsion-based hydrogel formulation of penciclovir for topical delivery. Int J Pharm. 2009;378(1–2):152–8.
24. Sahle FF, Metz H, Wohlrab J, Neubert RH. Polyglycerol fatty acid ester surfactant-based microemulsions for targeted delivery of ceramide AP into the stratum corneum: formulation, characterisation, *in vitro* release and penetration investigation. Eur J Pharm Biopharm. 2012;82(1):139–50.
25. Neubert R, Bendas C, Wohlrab W, Gienau B, Fürst W. A multilayer membrane system for modelling drug penetration into skin. Int J Pharm. 1991;75(1):89–94.
26. Constantinides PP, Scalart JP. Formulation and physical characterization of water-in-oil microemulsions containing long- *versus* medium-chain glycerides. Int J Pharm. 1997;158(1):57–68.
27. Hathout RM, Woodman TJ, Mansour S, Mortada ND, Geneidi AS, Guy RH. Microemulsion formulations for the transdermal delivery of testosterone. Eur J Pharm Sci. 2010;40(3):188–96.
28. Margulis-Goshen K, Netivi HD, Major DT, Gradzielski M, Raviv U, Magdassi S. Formation of organic nanoparticles from volatile microemulsions. J Colloid Interface Sci. 2010;342(2):283–92.
29. Kayali IH, Liu SH, Miller CA. Microemulsions containing mixtures of propoxylated sulfates with slightly branched hydrocarbon chains and cationic surfactants with short hydrophobes or PO chains. Colloids Surf, A Physicochem Eng Asp. 2010;354(1–3):246–51.
30. Lawrence MJ, Rees GD. Microemulsion-based media as novel drug delivery systems. Adv Drug Deliv Rev. 2000;45(1):89–121.
31. Date AA, Nagarsenker MS. Parenteral microemulsions: an overview. Int J Pharm. 2008;355(1–2):19–30.
32. Fanun M. Formulation and characterization of microemulsions based on mixed nonionic surfactants and peppermint oil. J Colloid Interface Sci. 2010;343(2):496–503.
33. Rojas O, Tiersch B, Frasca S, Wollenberger U, Koetz J. A new type of microemulsion consisting of two halogen-free ionic liquids and one oil component. Colloids Surf, A Physicochem Eng Asp. 2010;369(1–3):82–7.
34. Zech O, Thomaier S, Kolodziejski A, Touraud D, Grillo I, Kunz W. Ethylammonium nitrate in high temperature stable microemulsions. J Colloid Interface Sci. 2010;347(2):227–32.
35. Shukla A, Neubert RHH. Diffusion behavior of pharmaceutical O/W microemulsions studied by dynamic light scattering. Colloid Polym Sci. 2006;284(5):568–73.
36. Shukla A, Janich M, Jahn K, Neubert RHH. Microemulsions for dermal drug delivery studied by dynamic light scattering: effect of interparticle interactions in oil-in-water microemulsions. J Pharm Sci. 2003;92(4):730–8.
37. Gohy JF, Varshney SK, Jerome R. Water-soluble complexes formed by poly(2-vinylpyridinium)-block-poly(ethylene oxide) and poly(sodium methacrylate)-block-poly(ethylene oxide) copolymers. Macromolecules. 2001;34(10):3361–6.
38. Fanun M. Properties of microemulsions with mixed nonionic surfactants and citrus oil. Colloids Surf, A Physicochem Eng Asp. 2010;369(1–3):246–52.
39. Safavi A, Maleki N, Farjami F. Phase behavior and characterization of ionic liquids based microemulsions. Colloids Surf, A Physicochem Eng Asp. 2010;355(1–3):61–6.
40. Yu AH, Guo CY, Zhou YB, Cao FL, Zhu WW, Sun M, *et al.* Skin irritation and the inhibition effect on HSV-1 *in vivo* of penciclovir-loaded microemulsion. Int Immunopharmacol. 2010;10(10):1305–9.
41. Sharma G, Wilson K, van der Walle CF, Sattar N, Petrie JR, Ravi Kumar MN. Microemulsions for oral delivery of insulin: design, development and evaluation in streptozotocin induced diabetic rats. Eur J Pharm Biopharm. 2010;76(2):159–69.
42. Lin CC, Lin HY, Chen HC, Yu MW, Lee MH. Stability and characterisation of phospholipid-based curcumin-encapsulated microemulsions. Food Chem. 2009;116(4):923–8.
43. Saintruth H, Attwood D, Ktistis G, Taylor CJ. Phase studies and particle-size analysis of oil-in-water phospholipid microemulsions. Int J Pharm. 1995;116(2):253–61.
44. Trotta M, Cavalli R, Ugazio E, Gasco MR. Phase behaviour of microemulsion systems containing lecithin and lysolecithin as surfactants. Int J Pharm. 1996;143(1):67–73.
45. Kristl J, Volk B, Gasperlin M, Sentjurc M, Jurkovic P. Effect of colloidal carriers on ascorbyl palmitate stability. Eur J Pharm Sci. 2003;19(4):181–9.
46. Rozner S, Kogan A, Mehta S, Somasundaran P, Aserin A, Garti N, *et al.* Characterization of nonionic microemulsions by EPR. Part II. The effect of competitive solubilization of cholesterol and phytosterols on the nanostructure. J Phys Chem B. 2009;113(3):700–7.
47. Hemminga MA, Dries IJvd. Spin label applications to food science. In: Berliner LJ, editor. Bio Magn Re. 1998:345–7.
48. Bahri MA, Hoebeke M, Grammenos A, Delanaye L, Vandewalle N, Seret A. Investigation of SDS, DTAB and CTAB micelle microviscosities by electron spin resonance. Colloids Surf, A Physicochem Eng Asp. 2006;290(1–3):206–12.
49. Jadzyn J, Czechowski G, Stefaniak T. Viscosity of a series of 1,2-alkanediols. J Chem Eng Data. 2002;47(4):978–9.
50. Czechowski G, Jadzyn J. The viscous properties of diols. II. 1,2- and 1,5-pentanediol in water and 1-pentanol solutions. Z Naturforsch A. 2003;58(5–6):321–4.
51. Hou ZS, Li ZP, Wang HQ. Solubilization of poly(ethylene oxide) in sodium dodecyl sulfonate/octane/butanol/water reverse microemulsion. Colloids Surf, A Physicochem Eng Asp. 2000;168(2):109–13.
52. Zoumpanioti M, Stamatis H, Papadimitriou V, Xenakis A. Spectroscopic and catalytic studies of lipases in ternary hexane-1-propanol-water surfactantless microemulsion systems. Colloid Surf B. 2006;47(1):1–9.
53. Lucaciu CM, Dânsoreanu M, Damian G, Miclaus V. EPR study of the dynamics of some spin labels inclusion in cyclodextrins. Rom J Biophys. 2005;15(1–4):15–60.
54. Nakagawa K. EPR investigations of spin-probe dynamics in aqueous dispersions of a nonionic amphiphilic compound. J Am Oil Chem Soc. 2009;86(1):1–17.